

Modelization of charge carriers mobilities in halide perovskites : Fröhlich scattering and quantum localization effects in a dynamic disorder regime

Antoine Lacroix,^{1,*} Guy Trambly de Laissardière,^{2,†} Pascal Quémerais,^{1,‡} Jean-Pierre Julien,^{1,§} and Didier Mayou^{1,¶}

¹Université Grenoble Alpes, CNRS, Institut NEEL, F-38042 Grenoble, France

²Laboratoire de Physique Théorique et Modélisation, CNRS and Université de Cergy-Pontoise, 95302 Cergy-Pontoise, France

(Dated: March 18, 2022)

We analyze the quantum transport properties of MAPbI₃ within a tight-binding model. Charge carriers are strongly scattered by the Fröhlich interaction with longitudinal optical phonon modes. This limits their mobilities at room temperature to the order of 200 cm²/Vs. In the presence of additional extrinsic disorder the mobility decreases and a large fraction of the electronic states at band edges can be localized. These states would be insulating if the lattice were static, but their localization is broken by the dynamic disorder induced by the vibrations of the longitudinal optical modes. This process of electrons and holes diffusion, driven by the lattice dynamics, contributes to the unique electronic properties of this material.

PACS numbers: 72.10.-d, 72.15.Rn, 72.50.-i, 61.82.Fk

Metal halide perovskite have recently emerged as great materials for photovoltaic and optoelectronic devices^{1,2}. The rapid progresses obtained in these applications require also to gain a better fundamental understanding of their electronic properties. Therefore there is a need for improved theoretical models in particular for the electronic transport, and so far there is no consensus on a detailed theory of charge transport in these materials^{3,4}. Owing to their softness, the very low phonons frequency and the evidence for anharmonicity a strong dynamic thermal disorder develops at room temperature⁵⁻⁷. For a perfect crystal at room temperature theoretical investigations point toward the importance of the scattering of charge carriers by longitudinal optical (LO) phonon modes⁸. This coupling to LO modes could also lead to the formation of large polarons. Although the mass renormalization estimated to about 40 percent is moderate this polaronic effect is often considered in the literature⁹⁻¹¹. The dipolar moment of Methylammonium (MA) has also been considered as a possible source of scattering even though recent calculations suggest that the scattering by the associated dipolar field has a limited effect on transport¹². Other source of scattering have also been considered related to an anharmonic behavior of these crystals at room temperature¹³. Extrinsic disorder is of course present in real systems but its effect is also difficult to model.

In this letter we investigate the transport properties of electrons and holes in MAPbI₃ (MAPI) within a tight binding model which allows to perform all the calculations of electronic transport in real space¹⁴⁻¹⁷. We take into account the effect of intrinsic thermal disorder of the PbI₃ matrix as well as the dipolar field created by the MA cation. We use the recently introduced analytical Drude-Anderson model¹⁸ which is useful to interpret numerical or experimental results. From this model we extract the basic characteristics of the quantum transport such as scattering time, velocity correlation and backscattering effect which are at the heart of quantum localization. These results show that the polaronic state is not stable at room temperature and that the mobilities are determined mainly by the Fröhlich scattering and by quantum localization effects in a dynamic disorder regime. This dynamic disorder

tends to break the quantum localization by dephasing which allows charge carriers diffusion. This process of diffusion is neither a band like process nor a thermally activated hopping and contributes to the unique properties of this material.

We use a tight binding model approximation to describe our material. The Hamiltonian is written as:

$$\hat{H} = \sum_{i\mu\sigma} |i\mu\sigma\rangle \varepsilon_{i\mu} \langle i\mu\sigma| + \sum_{i\mu,j\mu',\sigma} |i\mu\sigma\rangle t_{i\mu,j\mu'} \langle j\mu'\sigma| + \sum_{i\mu\sigma,\mu'\sigma'} |i\mu\sigma\rangle \lambda_{i\mu\sigma,\mu'\sigma'} \langle i\mu'\sigma'|, \quad (1)$$

where $\varepsilon_{i\mu}$ is the onsite energy, of orbital μ on atom i , $t_{i\mu,j\mu'}$ is the hopping integral between orbitals μ on atom i and orbital μ' on a neighboring atom j , and $\lambda_{i\mu\sigma,\mu'\sigma'}$ is the spin orbit coupling between orbitals of the same atom, but of different spin σ and σ' . The orbitals participating in transport are the valence orbitals of each elements which are of s and p type. The MA molecule energy levels are too high compared to Lead and Iodine to participate in charge transport, and do not appear in the tight binding model, but they provide one electron per unit cell to the system. This type of Hamiltonian is very well suited for numerical studies. It can be separated in three parts, the diagonal elements, the off-diagonal elements, and the spin orbit elements. The tight binding parameters of the system without disorder have been fitted¹⁹ to be consistent with MAPI's *ab-initio* band structure calculations^{20,21}, and are used as a basis for this work.

We consider now the description of the intrinsic thermal disorder. The spin orbit coupling has a strong impact on MAPI's band structure, due to the splitting of the Lead p orbitals, but it is a local phenomenon and we assume that it is not affected by thermal disorder. So we only have to account for off-diagonal and diagonal disorder. MAPI's Debye temperature is around 175K²², much lower than room temperature, and we adopt a classical description for phonons since we focus mainly on room temperature properties.

The off-diagonal disorder is related to the distance and overlapping between orbitals. We describe the displacement of atoms using independent Einstein's oscillators. In this model, all atomic displacements are statistically independent,

and the potential is treated as harmonic and isotropic, even though the environment of I is not of cubic symmetry. Such single particle potentials have been computed from experimental data by Tyson et al.²³. For such a model, the distribution of atomic displacements is a gaussian centered on zero and of standard deviation $\sqrt{k_b T}/(\omega_0 \sqrt{m})$ where ω_0 is the pulsation, m is the atom's mass and $k_b T$ is the thermal energy. For Lead (*Pb*) $\hbar\omega_0 = 6.4$ meV and for Iodine (*I*) $\hbar\omega_0 = 5.4$ meV. Once an atomic configuration is set the hopping parameters are recomputed from the Slater-Koster relations²⁴ for changes in direction, and via a power law in $(d_0/d)^2$ for changes in distance from d_0 to the actual distance d .

The disorder of the onsite energies is determined by the electrical potential inside the material. The variation of this electrical potential with respect to the periodic structure is caused by the displacement of the charged ions and the orientation of the MA molecules. The contribution of the MA molecules to the diagonal disorder is found small¹² (see supplementary material), and has a negligible effect on mobilities. Therefore we present results only with diagonal disorder due to the displacement of Lead and Iodine ions. The displacement of an atom creates a dipole moment which is the product of the displacement by the Born charge in the considered direction. We use the Born charges computed by Prez-Osorio et al.⁶ for the Lead and Iodine atoms. The main contribution to the electrostatic potential is expected to come from the LO phonon modes, which energies are in the 10-13 meV range⁸. Here we also represent the statistics of the displacements by using an Einstein model of independent isolated atomic oscillators with an effective phonon pulsation ω_E close to 10 meV. We note that the phonon modes that contribute most to the diagonal disorder are the LO modes, which represent only a small portion of the complete set of modes^{8,25}, while the off diagonal disorder gets contribution from all modes. We thus assume that both disorders are statistically independent.

From the relation between the dipolar moments \vec{d}_i , $k_b T$ and ω_E , we find (see supplementary material) that the probability distribution of the dipoles is a Gaussian and that the variable $W = k_b T/(\epsilon_r \omega_E)^2$ is the parameter that determines the electrostatic potential statistics due to thermal disorder. In the rest of the paper we fix the temperature to $T = 300K$, the relative dielectric constant to $\epsilon_r = 5$ ²⁶. We find that the value of ω_E that reproduces best the gap at room temperature is close to 10 meV (see supplementary material) and discuss only the effect of varying ω_E around 10 meV. W increases when disorder increases, meaning that a decrease of ω_E corresponds to an increase of disorder. Finally we note that the exact structure and type of defects in MAPbI3 are not fully understood and some types of disorder that are not described in the present harmonic model could play a role. Yet the central idea of this work is that the transport properties are mainly determined by a single parameter, that describes the strength of disorder and the scattering rate. Here this parameter is ω_E (or W).

We first present results for $\omega_E = 10$ meV showing energy resolved analysis for the properties of electrons and holes. Figure 1 shows the density of states (DOS) $n(E)$, the occupied density of states $n(E)\exp(-\beta E)$, the mobility

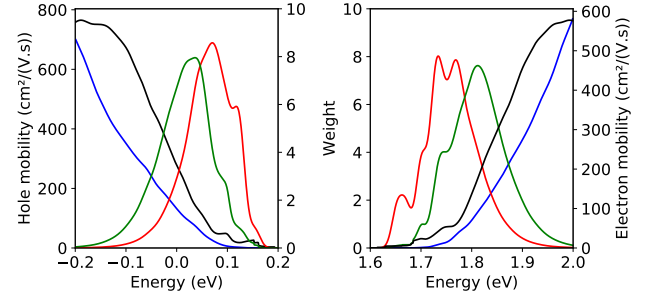


FIG. 1. (Color online) Variations of the carrier mobilities (black), the density of states (blue), the occupied DOS (red) and the differential conductivity (green) as a function of energy, near the band edges, for holes (**left**) and electrons (**right**). Except for the mobility the quantities are normalized (for each type of carrier) such that their integral is one on the represented energy interval (axis labeled weight)

$\mu(E)$ at energy E and the differential conductivity $d\sigma/dE = \mu(E)n(E)\exp(-\beta E)$. We find that the occupied DOS is important within a range of about 0.2eV and that states contributing the most to the transport of current are also within a range of about 0.2eV but slightly shifted away from the band edges. The very small mobility close to the band edge is related to the Urbach's tail, but it cannot be analyzed with the present energy resolution that is limited to 10 – 20 meV. The typical value of the mobility for states that contribute most is in the range 100-200 cm²/Vs which corresponds indeed to the best experimental mobilities. We note that results for electrons and holes are similar and in the rest of the paper we discuss only averaged properties of both charge carriers. Finally we note that the densities of states of both electrons and holes are very different from the parabolic shape typical of free particle with an effective mass. This indicates that the disorder in this model is strong and that the energy broadening of a state due to the disorder is comparable to its energy, counted from the band edge. According to the Ioffe-Regel criterion²⁷ one expects that quantum localization effects are important and we analyze now more precisely these quantum effects.

We start our discussion of the quantum localization effects by considering the Drude-Anderson model¹⁸ that was introduced recently and that fits very well the results of the present numerical study (see supplementary material for the fitted parameters). Two fundamental quantities for the quantum transport are the mean squared displacement $X^2(t)$ (that is computed through the RSKG method) and the velocity correlation function $C(t)$. They are defined for each type of carrier and are related by :

$$\frac{1}{2} \frac{dX^2(t)}{dt} = \int_0^t C(t') dt', \quad (2)$$

and the optical terahertz conductivity, $\sigma(\omega)$, (i.e. the real part of the full complex conductivity) can also be computed from $C(t)$ or $X^2(t)$ ^{18,28}. Using the Kubo formalism one can derive

$$\sigma(\omega) = e^2 n \frac{\tanh(\beta \hbar \omega / 2)}{\hbar \omega / 2} \text{Re} \int_0^\infty e^{i\omega t} C(t) dt, \quad (3)$$

where e and n are the charge and concentration for each carrier type. Thus the optical terahertz conductivity, contains informations about the charge carriers dynamics and the temporal behavior of the spreading of electronic states $X^2(t)$.

The Drude-Anderson model consists in assuming a phenomenological expression for the velocity correlation $C(t)$:

$$C(t) \simeq C_C e^{-t/\tau_C} - C_B e^{-t/\tau_B} e^{-t/\tau_\Phi}. \quad (4)$$

The first term on the right corresponds to the standard classical picture of electronic transport where scattering events lead to a loss of the memory of the initial velocity on a characteristic time τ_C . The second term on the right represents a negative contribution to the velocity correlation function. This corresponds to the backscattering phenomena which is at the heart of the Anderson localization phenomenon. Physically one must have $\tau_B > \tau_C$ because the backscattering phenomena occurs after several scattering events. The term e^{-t/τ_Φ} describes an exponential damping of the backscattering terms due to dephasing processes that do not conserve the charge carrier energy. In the present case the dephasing of the backscattering terms is due to the dynamics of the lattice and τ_Φ is of the order of the period of the LO modes, which are the main source of scattering, i.e. $\tau_\Phi \simeq 1/\omega_E$. In the following we shall discuss the results by considering mainly the time dependent and frequency dependent mobilities defined by :

$$\tilde{\mu}(t) = \frac{e}{k_b T} \frac{X^2(t)}{2t}, \quad \tilde{\mu}(\omega) = \frac{\sigma(\omega)}{ne}, \quad (5)$$

where $e > 0$ is the electron charge and the mobility μ is given by $\mu = \tilde{\mu}(t \rightarrow \infty) = \tilde{\mu}(\omega \rightarrow 0)$. We define also the static mobility μ_S and the classical mobility μ_C by :

$$\mu_S = \frac{e}{k_b T} (C_C \tau_C - C_B \tau_B), \quad \mu_C = \frac{e}{k_b T} (C_C \tau_C). \quad (6)$$

In the absence of dephasing i.e. by considering the lattice as static ($\tau_\Phi \rightarrow \infty$) one has $\mu = \mu_S$, and the ratio $R = \mu_S/\mu_C$ is an indicator of the importance of localization effects. Figure (2) shows the different regimes of diffusion and the corresponding optical conductivities. We consider typical regimes of diffusion : one which is classical and presents no localization effect ($R \simeq 1$), one which is strongly localized with ($R \simeq 0$), and two intermediate cases. At short time there is always a ballistic regime during which the charge carrier moves through the material without interacting with disorder i.e. $\tilde{\mu}(t) \propto t$. The end of this regime marks the elastic diffusion mean free time. This ballistic regime can be followed by a quantum diffusion regime which happens when disorder becomes strong enough so that charge carriers become localized, resulting in a drop in diffusivity and in mobility. Finally at sufficiently large time the diffusive regime is reached for which $X^2(t) \propto t$ and the diffusivity and the time dependent mobility $\tilde{\mu}(t)$ are constant. For a completely localized system $\tilde{\mu}(t)$ tends exactly to zero at

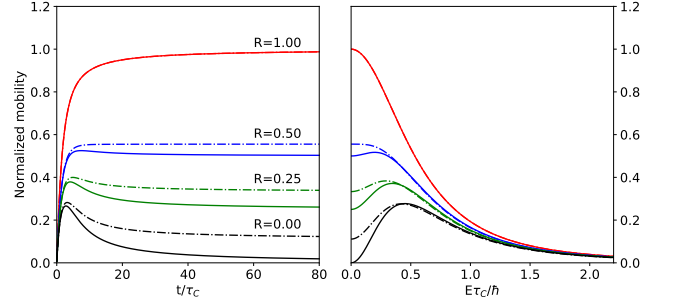


FIG. 2. (Color online) Normalized time dependent mobility $\tilde{\mu}(t)/\mu_C$ (left) and normalized frequency dependent mobility $\tilde{\mu}(\omega)/\mu_C$ (right) for different localization ratio $R = \mu_S/\mu_C$. The full line corresponds to results without dephasing processes and the dashed line corresponds to results with a dephasing process. Here $\tau_B = 2.5\tau_C$ and $\tau_\Phi = 8\tau_B$.

large times. Finally we emphasize that when the quantum localization increases the Drude peak is progressively replaced by a dip in the frequency dependent conductivity (figure (2) right panel).

In the presence of dephasing processes (i.e. for a finite τ_Φ), the mobility μ is the sum of a static contribution μ_S and of a contribution due to the lattice dynamics μ_{LD} with :

$$\mu = \mu_S + \mu_{LD}, \quad \mu_{LD} = \frac{e}{k_b T} \frac{L^2(\tau_\Phi)}{2\tau_\Phi}. \quad (7)$$

Since the dynamics of the lattice tends to break the effect of quantum localization μ_{LD} is positive with $L^2(\tau_\Phi) = 2C_B\tau_B^2/(1 + \tau_B/\tau_\Phi)$. In the classical limit there is no backscattering $C_B = 0$ and $\mu_{LD} = 0$. In the weak-localization regime there is some backscattering, and μ_{LD} gives a correction to the static mobility μ_S . In the strongly localized limit $\mu_S \simeq 0$ but transport is still possible thanks to the $\mu_{LD} > 0$ term, and in this limit $L^2(\tau_\Phi)$ is essentially equal to the localization length (see supplementary material). The physical picture is that the charge can diffuse up to a maximum extent which is the localization length. Then the diffusion stops and can start again only if a dephasing process breaks the electronic coherence. In this regime the diffusion coefficient is inversely proportional to the dephasing time. Thus the diffusion is driven by the lattice dynamics and indeed the diffusion coefficient increases linearly with the vibration frequency $\omega_E \propto 1/\tau_\Phi$. Let us emphasize that this regime where diffusion results from a dephasing process differs from the hopping regime at low temperature that is thermally activated. We note also that in this regime of lattice driven diffusion the mobility decreases when the temperature increases, just as in a band like conduction regime. Indeed increasing temperature and therefore static disorder decreases the localization length and $L^2(\tau_\Phi)$ without changing τ_Φ . From equation 7 this decreases μ_{LD} . The physical picture of the dephasing process corresponds to the so-called Thouless regime^{29–32} that is expected to occur near a metal-insulator transition. It is also equivalent to the concept of transient localization that has been proposed for crystalline organic semi-conductors like rubrene^{33–35}.

We come now to the study of charge carriers mobilities. By applying the RSKG (Real Space Kubo-Greenwood)^{14–17} method we perform a study of quantum transport without resorting to perturbative treatment of disorder. This method has been applied so far only to systems of one and two dimensions. The present calculation is the first application to a three dimensional system where we use systems containing several millions of unit cells. This opens new perspectives for the use of the RSKG method. Since holes and electrons have similar mobilities (see figure 1) we present values of the time dependent mobilities $\tilde{\mu}(t)$ and optical terahertz conductivities averaged over electrons and holes. The optical conductivity reflects the dynamics of the charge diffusion and could bring much information, but experimental results obtained so far appear somewhat contradictory^{36,37}. Further experimental studies are needed and could be compared to the present results.

The model with $\omega_E = 10$ meV is the one expected to be the closest to perfect bulk MAPI, $\omega_E = 12.5$ meV serving as a high expectation value, and $\omega_E = 7.5$ meV being used to describe a more imperfect MAPI sample with extrinsic disorder. The Drude-Anderson model fits the data of $\tilde{\mu}(t)$ very accurately which allows to derive its parameters from the numerical calculation of $X^2(t)$. We find that the LO phonon modes of MAPI limit the mobilities to maximum values of about $200 \text{ cm}^2/(\text{V.s})$ with μ_S and μ_{LD} contributions that are nearly equal. Even in this case of relatively high mobility quantum localization effects are strong with $R \simeq 0.15$. The elastic mean free path $l = \sqrt{\Delta X^2(\tau_C)}$ is about 20 \AA (resp. 30 \AA) for $\omega_E = 10$ meV (resp. $\omega_E = 12.5$ meV). The scattering times τ_C are about 8.3 (resp. 10.3) Femtoseconds for $\omega_E = 10$ meV (resp. $\omega_E = 12.5$ meV). As expected the backscattering times τ_B are 2-3 times larger than τ_C (see supplementary material).

The results for $\omega_E = 7.5$ meV show the quick increase of the quantum localization with additional disorder ($R \simeq 0.03$). The scattering time is $\tau_C \simeq 2.6$ Femtoseconds and a large portion of the charge carriers states close to the band edges are strongly localized on a time scale $\tau_B \simeq 8$ Femtoseconds, which is short compared to the phonon period (of about 400 Femtoseconds). Figure (3) shows that for this disorder the mobility is of the order of $\mu \simeq 50 \text{ cm}^2/\text{V.s}$ with $\mu_S \simeq 10 \text{ cm}^2/\text{V.s}$ and $\mu_{LD} \simeq 40 \text{ cm}^2/\text{V.s}$. Therefore in this regime the mobility is dominated by the contribution due to the lattice dynamics. We note that the RSKG method tends to underestimate the localization so that for these parameters the total mobility should have an even lower relative contribution from the static mobility.

These results allow to discuss the formation of large polarons at room temperature. The coupling constant $\alpha \simeq 2 - 3$ implies the formation of large polarons at low temperatures. The formation energy of the polaron is given by $E_{Pol} \simeq \alpha \hbar \omega_E \simeq 30 \text{ meV}$ ^{10,11}. Yet in the high temperature limit, i.e. above the Debye temperature (175 K in MAPI²²), the phonon modes are thermally excited and this induces a scattering of electrons and a tendency to erase the polaronic state. This is shown for example by recent theoretical calculations in the case of CsPbBr₃³⁸. This scattering remains delicate to compute with standard polaron theories^{39,40}. The scattering by thermal vibrations induces an energy broadening

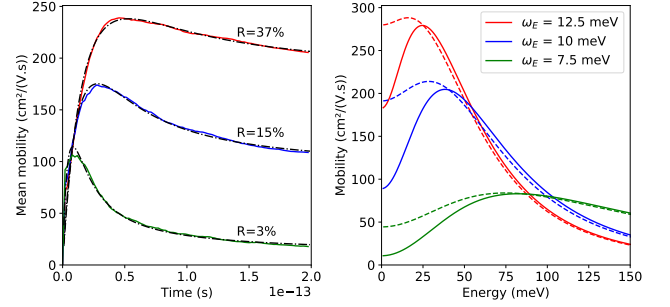


FIG. 3. (Color online) Mobilities averaged over hole and electron states. **Left** Mobility as a function of time for different values of ω_E (full line), and the corresponding fits using the Drude-Anderson model (black dashed line). The ratio $R = \mu_S/\mu_C$ is obtained from the fitted parameters. **Right** Mobilities as a function of frequency calculated from the Drude-Anderson model. Without dephasing processes (full line) and with dephasing (dotted line). The zero energy mobility is equal to μ_S (without dephasing) or $\mu_S + \mu_{LD}$ (with dephasing). The dephasing time is $\tau_\phi = 7.10^{-14} \text{ s}$.

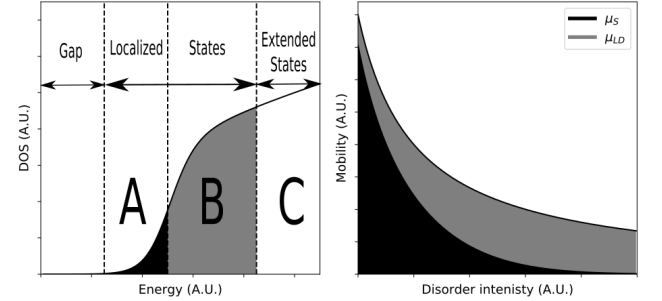


FIG. 4. **Left**: Schematic representation of the different type of states as a function of energy. Region A : diffusion dominated by thermally activated hopping. Region B : diffusion is through the dephasing processes induced by the lattice dynamics. Region C : band-like diffusion. **Right**: Schematic representation of the evolution of the mobility $\mu = \mu_S + \mu_{LD}$ as a function of disorder. Static contribution μ_S (black) and lattice driven mobility μ_{LD} (grey) are shown.

$\Delta E \simeq \hbar/\tau$ where τ is the electron lifetime due to scattering. In our case due to the long range nature of the scattering by longitudinal modes there is forward scattering and $\tau \leq \tau_C$. Then for the systems with highest mobility $\mu \simeq 200 \text{ cm}^2/\text{V.s}$ the energy broadening is $\Delta E \geq \hbar/\tau_C \geq 90 \text{ meV}$. Therefore even for this less disordered cases the energy broadening due to the Fröhlich scattering is larger than the polaron formation energy $\Delta E > E_{Pol}$. Correlatively the estimated polaron radius of about $40\text{-}50 \text{ \AA}$ is larger than the elastic mean free-path which is less than $20\text{-}30 \text{ \AA}$. This indicates that because of the moderate coupling constant $\alpha \simeq 2 - 3$ the polaron state is erased by the strong disorder that exists well above the Debye temperature, at room temperature. This justifies the present model that consist, in a first step, to neglect at high temperature the action of the charge carrier on the lattice and just retain the action of the lattice on the charge carrier.

Figure (4) summarizes the scenario that is supported by the

present study. If we consider first an instantaneous configuration of disorder there are extended states, in region C, that are separated by a mobility edge from localized states, in regions B and A. However due to the dynamic disorder even the localized states can get a finite mobility. For states closest from the mobility edge (region B), this mobility is induced by the dephasing process described in this paper. Farther from the mobility edge (region C) one expects that the diffusion will be dominated by thermally activated hopping as is usual in disordered systems. We suggest that the small Urbach energy ($E_U \leq 15\text{meV}$) that is measured in MAPbI₃ could be related to this region C. The right panel of figure (4) shows a qualitative behavior of the mobility μ and of its static μ_S and dynamic μ_{LD} components when disorder increases.

To conclude this work shows that electrons and holes in MAPbI₃ have similar transport properties. We showed that the polaronic state is not stable at room temperature and that the dominant effect is that of Fröhlich scattering of electrons and holes. We expect that other effects like dipolar field of MA cation or other source of distortion of the lattice are less important. The emerging picture is that of strong quantum lo-

calization effects due to the Fröhlich scattering or to extrinsic disorder. The quantum localization that we predict in MAPbI₃ can appear experimentally similar to a polaronic effect but it is induced by the strong potential disorder. The maximum mobility at room temperature is about $200\text{ cm}^2/(\text{V.s})$ and we find that for mobilities below $\mu_c \simeq 50\text{ cm}^2/(\text{V.s})$ the electronic diffusion is mainly due to the dynamic disorder. In this process states that are localized by the static disorder can diffuse thanks to the dephasing process induced by the dynamic disorder. This differs from the hopping conduction which is a thermally activated process. We suggest that this mechanism of electronic diffusion induced by the lattice dynamics, which has rarely been observed in inorganic semi-conductors, could be observed more frequently in soft materials like for example crystalline organic semi-conductors or hybride perovskites.

We acknowledge fruitful discussions with many colleagues and wish to thank Jacky Even, Claudine Katan, Paulina Plochocka, Julien Delahaye, Dang Le-Si, and Gabriele Davino. We also thank Ghassen Jemai and Kevin-Davis Richler for their help during this study.

* antoine.lacroix@neel.cnrs.fr

† guy.trambly@u-cergy.fr

‡ pascal.quemerais@neel.cnrs.fr

§ jean-pierre.julien@neel.cnrs.fr

¶ didier.mayou@neel.cnrs.fr

¹ Martin A. Green, Anita Ho-Baillie, and Henry J. Snaith, “The emergence of perovskite solar cells,” *Nature Photonics* **8**, 506 EP – (2014), review Article.

² Joseph S. Manser, Jeffrey A. Christians, and Prashant V. Kamat, “Intriguing optoelectronic properties of metal halide perovskites,” *Chemical Reviews* **116**, 12956–13008 (2016), pMID: 27327168, <https://doi.org/10.1021/acs.chemrev.6b00136>.

³ Lucy D. Whalley, Jarvist M. Frost, Young-Kwang Jung, and Aron Walsh, “Perspective: Theory and simulation of hybrid halide perovskites,” *The Journal of Chemical Physics* **146**, 220901 (2017), <https://doi.org/10.1063/1.4984964>.

⁴ Chol-Jun Yu, “Advances in modelling and simulation of halide perovskites for solar cell applications,” *Journal of Physics: Energy* **1**, 022001 (2019).

⁵ Lucy D. Whalley, Jonathan M. Skelton, Jarvist M. Frost, and Aron Walsh, “Phonon anharmonicity, lifetimes, and thermal transport in $\text{CH}_3\text{NH}_3\text{PbI}_3$ from many-body perturbation theory,” *Phys. Rev. B* **94**, 220301 (2016).

⁶ Miguel A. Prez-Osorio, Rebecca L. Milot, Marina R. Filip, Jay B. Patel, Laura M. Herz, Michael B. Johnston, and Feliciano Giustino, “Vibrational properties of the organotinorganic halide perovskite $\text{CH}_3\text{NH}_3\text{PbI}_3$ from theory and experiment: Factor group analysis, first-principles calculations, and low-temperature infrared spectra,” *The Journal of Physical Chemistry C* **119**, 25703–25718 (2015), <https://doi.org/10.1021/acs.jpcc.5b07432>.

⁷ M. Baranowski, J. M. Urban, N. Zhang, A. Surrente, D. K. Maude, Zahra Andaji-Garmaroudi, S. D. Stranks, and P. Plochocka, “Static and dynamic disorder in triple-cation hybrid perovskites,” *The Journal of Physical Chemistry C* **122**, 17473–17480 (2018), <https://doi.org/10.1021/acs.jpcc.8b05222>.

⁸ Adam D. Wright, Carla Verdi, Rebecca L. Milot, Giles E. Eperon, Miguel A. Pérez-Osorio, Henry J. Snaith, Feliciano Giustino,

Michael B. Johnston, and Laura M. Herz, “Electron-phonon coupling in hybrid lead halide perovskites,” *Nature Communications* **7**, 11755 EP – (2016), article.

⁹ Amanda J. Neukirch, Wanyi Nie, Jean-Christophe Blancon, Kanatassen Appavoo, Hsinhan Tsai, Matthew Y. Sfeir, Claudine Katan, Laurent Pedesseau, Jacky Even, Jared J. Crochet, Gautam Gupta, Aditya D. Mohite, and Sergei Tretiak, “Polaron stabilization by cooperative lattice distortion and cation rotations in hybrid perovskite materials,” *Nano Letters* **16**, 3809–3816 (2016), pMID: 27224519, <https://doi.org/10.1021/acs.nanolett.6b01218>.

¹⁰ Jarvist Moore Frost, Lucy D. Whalley, and Aron Walsh, “Slow cooling of hot polarons in halide perovskite solar cells,” *ACS Energy Letters* **2**, 2647–2652 (2017), pMID: 29250603, <https://doi.org/10.1021/acsenenergylett.7b00862>.

¹¹ Christoph Wolf, Himchan Cho, Young-Hoon Kim, and Tae-Woo Lee, “Polaronic charge carrier lattice interactions in lead halide perovskites,” *ChemSusChem* **10**, 3705–3711 (2017), <https://onlinelibrary.wiley.com/doi/pdf/10.1002/cssc.201701284>.

¹² Luigi Martiradonna, “Riddles in perovskite research,” *Nature Materials* **17**, 377–377 (2018).

¹³ Wei Li, Andrey S. Vasenko, Jianfeng Tang, and Oleg V. Prezhdo, “Anharmonicity extends carrier lifetimes in lead halide perovskites at elevated temperatures,” *The Journal of Physical Chemistry Letters* **10**, 6219–6226 (2019), pMID: 31556621, <https://doi.org/10.1021/acs.jpcclett.9b02553>.

¹⁴ D. Mayou, “Calculation of the conductivity in the short-mean-free-path regime,” *EPL (Europhysics Letters)* **6**, 549 (1988).

¹⁵ D. Mayou and S. Khanna, “A Real-Space Approach to Electronic Transport,” *Journal de Physique I* **5**, 1199–1211 (1995).

¹⁶ S. Roche and D. Mayou, “Conductivity of quasiperiodic systems: A numerical study,” *Phys. Rev. Lett.* **79**, 2518–2521 (1997).

¹⁷ François Triozon, Julien Vidal, Rémy Mosseri, and Didier Mayou, “Quantum dynamics in two- and three-dimensional quasiperiodic tilings,” *Phys. Rev. B* **65**, 220202 (2002).

¹⁸ S. Fratini, S. Ciuchi, and Didier Mayou, “Phenomenological model for charge dynamics and optical response of disordered systems: Application to organic semiconductors,” *Physical Re-*

- view B **89** (2014), 10.1103/PhysRevB.89.235201.
- 19 Soline Boyer-Richard, Claudine Katan, Boubacar Traor, Reinhard Scholz, Jean-Marc Jancu, and Jacky Even, "Symmetry-based tight binding modeling of halide perovskite semiconductors," *The Journal of Physical Chemistry Letters* **7**, 3833–3840 (2016), pMID: 27623678, <https://doi.org/10.1021/acs.jpclett.6b01749>.
 - 20 Federico Brivio, Keith T. Butler, Aron Walsh, and Mark van Schilfgaarde, "Relativistic quasiparticle self-consistent electronic structure of hybrid halide perovskite photovoltaic absorbers," *Phys. Rev. B* **89**, 155204 (2014).
 - 21 Towfiq Ahmed, C. La o vorakiat, T. Salim, Y. M. Lam, Elbert E. M. Chia, and Jian-Xin Zhu, "Optical properties of organometallic perovskite: An ab initio study using relativistic GW correction and bethe-salpeter equation," *EPL (Europhysics Letters)* **108**, 67015 (2014).
 - 22 Jing Feng, "Mechanical properties of hybrid organic-inorganic $\text{ch}_3\text{nh}_3\text{b}_3\text{x}_3$ (b = sn, pb; x = br, i) perovskites for solar cell absorbers," *APL Materials* **2**, 081801 (2014), <https://doi.org/10.1063/1.4885256>.
 - 23 T. A. Tyson, W. Gao, Y.-S. Chen, S. Ghose, and Y. Yan, "Large thermal motion in halide perovskites," *Scientific Reports* **7**, 9401 (2017).
 - 24 J. C. Slater and G. F. Koster, "Simplified lcao method for the periodic potential problem," *Phys. Rev.* **94**, 1498–1524 (1954).
 - 25 Federico Brivio, Jarvist M. Frost, Jonathan M. Skelton, Adam J. Jackson, Oliver J. Weber, Mark T. Weller, Alejandro R. Goñi, Aurélien M. A. Leguy, Piers R. F. Barnes, and Aron Walsh, "Lattice dynamics and vibrational spectra of the orthorhombic, tetragonal, and cubic phases of methylammonium lead iodide," *Phys. Rev. B* **92**, 144308 (2015).
 - 26 Federico Brivio, Keith T. Butler, Aron Walsh, and Mark van Schilfgaarde, "Relativistic quasiparticle self-consistent electronic structure of hybrid halide perovskite photovoltaic absorbers," *Phys. Rev. B* **89**, 155204 (2014).
 - 27 S. E. Skipetrov and I. M. Sokolov, "Ioffe-regel criterion for anderson localization in the model of resonant point scatterers," *Phys. Rev. B* **98**, 064207 (2018).
 - 28 S. Fratini, S. Ciuchi, D. Mayou, G. Trambly de Laissardière, and A. Troisi, "A map of high-mobility molecular semiconductors," *Nature Materials* **16**, 998–1002 (2017).
 - 29 Yoseph Imry, "Possible role of incipient anderson localization in the resistivities of highly disordered metals," *Phys. Rev. Lett.* **44**, 469–471 (1980).
 - 30 J Delahaye, C Berger, and G Fourcaudot, "Thouless and critical regimes in insulating icosahedral AlPdRe ribbons," *Journal of Physics: Condensed Matter* **15**, 8753–8766 (2003).
 - 31 Z Ovadyahu, "Some finite temperature aspects of the anderson transition," *Journal of Physics C: Solid State Physics* **19**, 5187–5213 (1986).
 - 32 Julien Delahaye and Claire Berger, "The question of intrinsic origin of the metal-insulator transition in i-alpdre quasicrystal," *The European Physical Journal B* **88**, 102 (2015).
 - 33 S. Ciuchi, S. Fratini, and D. Mayou, "Transient localization in crystalline organic semiconductors," *Phys. Rev. B* **83**, 081202 (2011).
 - 34 Simone Fratini, Didier Mayou, and Sergio Ciuchi, "The transient localization scenario for charge transport in crystalline organic materials," *Advanced Functional Materials* **26**, 22922315 (2016).
 - 35 Ahmed Missaoui, Jouda Khabthani, Guy Trambly de Laissardière, and Didier Mayou, "Two-dimensional electronic transport in rubrene: the impact of inter-chain coupling," (2019).
 - 36 Liang Luo, Long Men, Zhaoyu Liu, Yaroslav Mudryk, Xin Zhao, Yongxin Yao, Joong M. Park, Ruth Shinar, Joseph Shinar, Kai Ming Ho, Ilias E. Perakis, Javier Vela, and Jigang Wang, "Ultrafast terahertz snapshots of excitonic rydberg states and electronic coherence in an organometal halide perovskite," *Nature Communications* **8**, 15565 EP – (2017), article.
 - 37 David A. Valverde-Chvez, Carlito S. Ponseca, Constantinos C. Stoumpos, Arkady Yartsev, Mercouri G. Kanatzidis, Villy Sundström, and David G. Cooke, "Intrinsic femtosecond charge generation dynamics in single crystal $\text{ch}_3\text{nh}_3\text{pb}_3\text{i}_3$," *Energy Environ. Sci.* **8**, 3700–3707 (2015).
 - 38 Marco Bernardi, Private communication.
 - 39 F.M. Peeters and J.T. Devreese, "Theory of polaron mobility," (Academic Press, 1984) pp. 81 – 133.
 - 40 Jarvist Moore Frost, "Calculating polaron mobility in halide perovskites," *Phys. Rev. B* **96**, 195202 (2017).
 - 41 Christopher Grote and Robert F. Berger, "Strain tuning of tinhalide and leadhalide perovskites: A first-principles atomic and electronic structure study," *The Journal of Physical Chemistry C* **119**, 22832–22837 (2015), <https://doi.org/10.1021/acs.jpcc.5b07446>.
 - 42 Rohit Prasanna, Aryeh Gold-Parker, Tomas Leijtens, Bert Conings, Aslihan Babayigit, Hans-Gerd Boyen, Michael F. Toney, and Michael D. McGehee, "Band gap tuning via lattice contraction and octahedral tilting in perovskite materials for photovoltaics," *Journal of the American Chemical Society* **139**, 11117–11124 (2017), pMID: 28704048, <https://doi.org/10.1021/jacs.7b04981>.
 - 43 Sharada Govinda, Bhushan P. Kore, Menno Bokdam, Pratibha Mahale, Abhinav Kumar, Somnath Pal, Biswajit Bhattacharyya, Jonathan Lahnsteiner, Georg Kresse, Cesare Franchini, Anshu Pandey, and D. D. Sarma, "Behavior of methylammonium dipoles in mapbx_3 (x = br and i)," *The Journal of Physical Chemistry Letters* **8**, 4113–4121 (2017), pMID: 28812901, <https://doi.org/10.1021/acs.jpclett.7b01740>.
 - 44 Nathaniel P. Gallop, Oleg Selig, Giulia Giubertoni, Huib J. Bakker, Yves L. A. Rezus, Jarvist M. Frost, Thomas L. C. Jansen, Robert Lovrincic, and Artem A. Bakulin, "Rotational cation dynamics in metal halide perovskites: Effect on phonons and material properties," *The Journal of Physical Chemistry Letters* **9**, 5987–5997 (2018), <https://doi.org/10.1021/acs.jpclett.8b02227>.

Appendix A: Drude-Anderson Model

1. General relations

One of the focus of our work has been the computation of the mean squared displacement of charge carrier as a function of time and energy, $X^2(E, t)$. In our formalism this quantity is defined as

$$X^2(E, t) = \frac{\text{Tr}([\hat{X}(t) - \hat{X}(0)]^2 \delta(E - \hat{H}))}{\text{Tr}(\delta(E - \hat{H}))}. \quad (\text{A1})$$

We then compute the thermodynamic average over the density of states as

$$X^2(t) = \frac{\int_0^\infty n(E) e^{-\beta(E-\mu)} X^2(E, t) dE}{\int_0^\infty n(E) e^{-\beta(E-\mu)} dE}, \quad (\text{A2})$$

which gives us the average spread through the lattice of a thermally distributed population of charge carriers, and simply relates to the classical diffusion coefficient D and mobility μ ,

$$D = \lim_{t \rightarrow \infty} \frac{X^2(t)}{2t}, \quad (\text{A3})$$

$$\mu = \frac{eD}{k_B T}. \quad (\text{A4})$$

Another value of interest, which behaviour we are able to model more easily is the velocity self correlation function as a function of time, $C(t)$, which is defined as

$$C(t) = \frac{1}{2} \langle \hat{V}_x(t) \hat{V}_x(0) + \hat{V}_x(0) \hat{V}_x(t) \rangle. \quad (\text{A5})$$

It represents the correlation that exist between the velocity of a charge carrier at time t and it's initial velocity at $t = 0$. This quantity is directly related to the diffusion processes at play in the material. $C(t)$ and $X^2(t)$ are related as

$$\frac{dX^2(t)}{2dt} = \int_0^t C(t') dt'. \quad (\text{A6})$$

From them we can derive formulas for the conductivity, depending on what is more convenient one can use any of the following forms,

$$\sigma(\omega) = ne^2 \frac{\tanh(\beta \hbar \omega / 2)}{\hbar \omega / 2} \text{Re} \int_0^\infty e^{i\omega t} C(t) dt = ne\mu(\omega), \quad (\text{A7})$$

$$\sigma(\omega) = -ne^2 \omega^2 \frac{\tanh(\beta \hbar \omega / 2)}{\hbar \omega} \text{Re} \int_0^\infty e^{i\omega t} X^2(t) dt, \quad (\text{A8})$$

The correlation function at time $t = 0$ is classically related to the effective mass and the temperature as

$$C(0) = \langle V(0)^2 \rangle = \frac{k_B T}{m^*} \simeq 2,3 \cdot 10^{14} \text{ cm}^2 / \text{s}^2, \quad (\text{A9})$$

for an effective mass $m^* = 0.2me$.

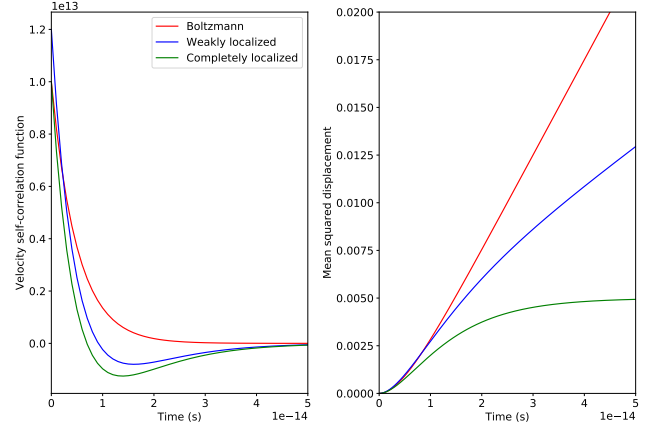


FIG. 5. (Color online) **Left:** Velocity self-correlation function as a function of time for different regimes. **Right:** Corresponding mean squared displacement as function of time.

2. Approximation of the Drude-Anderson model

The shape of $C(t)$ is directly related to the interaction charge carrier have with the lattice. Drude's model of electronic transport considers non interacting electrons, moving through the material via successive collisions with the much more massive and thus immobile atoms. The average time between collisions is τ and thus the probability for an electron to undergo a collision is

$$dP = \frac{dt}{\tau}. \quad (\text{A10})$$

One of Drude's approximation is that, after a collision, electrons completely loose the memory of their initial velocity, thus the velocity after the collision is not correlated to the one before. The evolution over time of self-correlation function of the velocity, $C(t)$, is thus directly proportional to the probability of collision, and we have

$$\frac{dC(t)}{dt} = C(t) \frac{dP}{dt} = -\frac{C(t)}{\tau}. \quad (\text{A11})$$

and thus

$$C(t) = C e^{-t/\tau}, \quad (\text{A12})$$

With $\hat{V}_x(t) = d\hat{X}(t)/dt$. The Drude-Anderson model builds upon the Drude model by adding the possibility for electron to backscatter, creating negative correlation with the original velocity after multiple collisions. This corresponds to backscattering which is at the heart of the Anderson localization phenomenon. Thus appears a negative correlation term for characteristic time $\tau_B > \tau_C$:

$$C(t) = C_C e^{-t/\tau_C} - C_B e^{-t/\tau_B} e^{-t/\tau_C}, \quad (\text{A13})$$

$\omega_E(\text{meV})$	$C_C(10^{15}\text{m}^2/\text{s}^2)$	$\tau_C(\text{fs})$	$C_B(10^{15}\text{m}^2/\text{s}^2)$	$\tau_B(\text{fs})$
12.5	1.23	10.3	0.25	31.4
10	1.82	8.28	0.7	18.3
7.5	3.37	2.56	1.02	8.16

TABLE I. Drude-Anderson parameters obtained for the different values of ω_E studied.

Where C_D and τ_C relate to the classical diffusion behaviour, and C_B and τ_B relate to the backscattering phenomenon, and τ_ϕ describes the effect the de-phasing processes, in our case the LO phonons, have on localization. These dephasing effects can be seen simply as a renormalization of τ_B .

3. Diffusion and conduction in the Drude-Anderson model

Combining this form with A6 gives analytical forms to $X^2(t)$, μ , $\sigma(\omega)$, and the localization length L_{LOC} :

$$\frac{\Delta X^2(t)}{2} = C_C \tau_C^2 (e^{-t/\tau_C} - 1) - C_B \tau_B^2 (e^{-t/\tau_B} - 1) + t(C_C \tau_C - C_B \tau_B), \quad (\text{A14})$$

$$L_{LOC}^2 = 2(C_B \tau_B^2 - C_C \tau_C^2) = 2C_B \tau_B^2 (1 - \frac{\tau_C}{\tau_B}) \quad (\text{A15})$$

$$\mu = \frac{e}{k_B T} (C_C \tau_C - C_B \tau_B) \quad (\text{A16})$$

$$\sigma(\omega) = ne^2 \frac{\tanh(\beta \hbar \omega / 2)}{\hbar \omega / 2} \left(\frac{C_C \tau_C}{\omega^2 \tau_C^2 + 1} - \frac{C_B \tau_B}{\omega^2 \tau_B^2 + 1} \right). \quad (\text{A17})$$

Note that we always have $C_C \tau_C \geq C_B \tau_B$ and $\tau_C \leq \tau_B$ and as such $\sigma(\omega)$ is always positive. In the case of non localized electrons, $C_B = 0$, and in the case of electrons completely localized at long times, we have $C_C \tau_C = C_B \tau_B$.

Surprisingly the Drude model which totally neglects quantum localization and the present calculations predict comparable scattering times of the order of 10^{-14}s for mobilities in the range of $100\text{cm}^2/\text{Vs}$. This is related to the fact that the strong electrostatic disorder has two opposite effects. On one hand the disorder scatters strongly the states and tends to localize them but on the other hand it leads to a strong mixing of states at band edges with states away from band edges which have a much larger average square velocity. This increased average square velocity strongly increases the quantum diffusion at short times. This is shown by the coefficient $C_C \simeq 1.82 \cdot 10^{15}\text{cm}^2/\text{s}^2$ (see Table I), which is much higher than found in the Drude model $C_D \simeq 2,3 \cdot 10^{14}\text{cm}^2/\text{s}^2$ (see above equation A9), and tends to increase when disorder increases.

Appendix B: Modelization of disorder and Impact of the Methyl-ammonium molecule

1. Parameter W for the statistical distribution of potential

We consider first the distribution for electrostatic potential. On a given site 0 the potential is the sum of potentials created by the various dipoles. We note $i = (k, l)$ the global index that represents the site k and the component l of the dipole.

$$V(0) = \sum_i \frac{1}{4\pi\epsilon_0\epsilon_r} \frac{q_i \vec{d}_i \cdot \vec{r}_i}{r_i^3} \quad (\text{B1})$$

We define a rescaled atomic displacement $\vec{D}_i = \vec{d}_i / \epsilon_r$ then :

$$V(0) = \sum_i \frac{1}{4\pi\epsilon_0} \frac{q_i \vec{D}_i \cdot \vec{r}_i}{r_i^3} \quad (\text{B2})$$

Using the stiffness at site i : $k_i = m_i \omega_E^2$ the probability distribution for \vec{D}_i is

$$P_i \propto \exp(-1/2 k_i d_i^2 / k_B T) \propto \exp(-1/2 m_i \omega_E^2 \epsilon_r^2 D_i^2 / k_B T) \quad (\text{B3})$$

with $W = k_B T / (\omega_E^2 \epsilon_r^2)$

$$P_i \propto \exp(-1/2 m_i D_i^2 / W) \quad (\text{B4})$$

Therefore the probability distribution of the dipoles depends only on the parameter $W = k_B T / (\omega_E^2 \epsilon_r^2)$.

2. Band gap and parameter ω_E

The variation of the hopping integrals due to atomic motion is found to be significant, of the order of 20% on average. Although we find that this disorder has little effect on charge carriers mobility, it has a sizable effect on the band-gap of MAPI and tends to increase it from 1.6eV (i.e. the value for the perfect periodic lattice) to 1.8eV. This increase of the gap is reminiscent of what happens with some distortions or tilts of the octahedrons^{41,42}. This effect tends to be compensated at room temperature by the diagonal disorder. The LO phonons are the source of strong electrostatic potential variation in the material, of the order of 0.5eV and their impact on charge carrier mobilities is considerable. Using the atomic potentials of²³ as basis for the motion of atoms, and imposing the band-gap to be 1.6 eV at room temperature, we find that the value of ω_E for this model is close to 10 meV.

3. Impact of the MA cation on mobilities

We have studied the impact of the MA molecule and compared it to that of the LO phonon modes. We consider a dipole

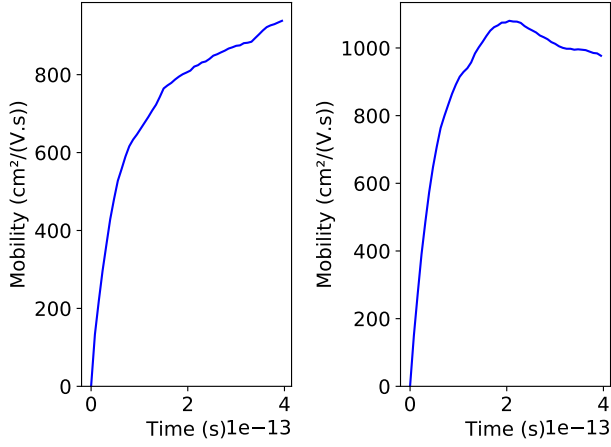


FIG. 6. Thermodynamically averaged mobilities as a function of time for holes (left) and electron (right) for a sample containing only MA molecules disorder.

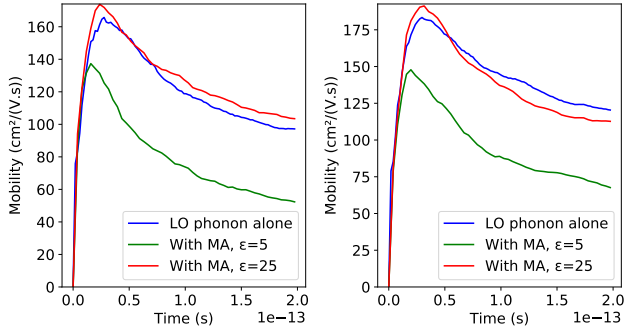


FIG. 7. (Color online) Thermodynamically averaged mobilities for holes (left) and electrons (right) for different combinations of disorder. Previously shown mobilities results for LO phonons with $\omega_E = 10$ are shown in blue, and results obtained when adding the MA molecules with different ϵ_r are shown in green ($\epsilon_r = 5$) and red ($\epsilon_r = 25$).

moment of the MA molecule of $2.1D$ and neglect the corre-

lation in orientation between neighbouring molecules^{43,44}. In the case of the MA molecule alone, without disorder from the LO phonon, and in the worst case scenario of $\epsilon_r = 5$, we found that they limit the charge carrier mobilities from around 900 to $1000 \text{ cm}^2/(\text{V.s})$, in concordance with other studies¹².

When looking at the system with both LO phonons and MA molecules, one need to consider the characteristic times of these phenomenon. The LO phonon motion happen on time constants of $0.5ps$ while the MA molecules have much bigger time constant of around $10ps$. As such the MA molecules are screened by the phonons and the dielectric permittivity associated is expected to be much bigger than 5, up to 25. We present both cases of $\epsilon_r = 5$ and $\epsilon_r = 25$. We find that in the worst case (see Figure 7), MA molecules have a weak effect on mobilities, and in the most realistic case, have nearly no effect. It is interesting to note however, that in a classical scenario, when adding disorder of the LO phonon with MA, one would expect to have the relations :

$$\frac{1}{\tau} = \frac{1}{\tau_{LO}} + \frac{1}{\tau_{MA}}, \quad (\text{B5})$$

$$\frac{1}{\mu} = \frac{1}{\mu_{LO}} + \frac{1}{\mu_{MA}}. \quad (\text{B6})$$

Considering the mobilities obtained for the disorder separated from one another (see Figures 6 and 7), this classical relation predicts mobilities of around $90 \text{ cm}^2/(\text{V.s})$, which is higher than mobilities of $50 \text{ cm}^2/(\text{V.s})$ computed in Figure 7. This reinforces the idea that quantum interferences play a major role in MAPI, and that the addition of even small quantities of disorder to the system tends to quickly localize charge carriers, and the need for a model that goes beyond the semi-classical limit.

Furthermore, the addition of the MA molecules can be seen as a widening of onsite energies distribution. This widening is well fitted by decreasing the LO phonon energy from $\omega_E = 10 \text{ meV}$ to 9.25 meV . As such, the MA molecules have for effect, at best, a renormalization of ω_E from the point of view of transport. Because we chose the value $\omega_E = 10 \text{ meV}$ to fit the bandgap of 1.6 eV , we believe our value already encases the effect of the MA molecules.